Economic Geology
Vol. 96, 2001, pp. 75–89

Timing of Gold and Arsenic Sulfide Mineral Deposition at the Getchell Carlin-Type Gold Deposit, North-Central Nevada

Jean S. Cline[†]

University of Nevada, Las Vegas, 4505 Maryland Parkway, Box 454010, Las Vegas, Nevada 89154-4010

Abstract

Pregold mineralization at the Getchell Carlin-type gold deposit includes quartz and base metal vein mineralization associated with intrusion of a Cretaceous granodiorite stock. The veins contain minor pyrite and trace chalcopyrite, arsenopyrite, galena, and sphalerite. The pyrite is moderately coarse and, in thin section, has high relief, is well polished, and is fractured and locally cemented by the gold ore assemblage. White micas are associated with veins near the granodiorite intrusion. Gold was not observed or detected by fire assay analyses of samples or electron microprobe analyses of pyrites. Microprobe analyses show that pregold pyrites have near-stoichiometric compositions. Variable, low arsenic is present in pyrite in samples overprinted by gold mineralization. Secondary ion mass spectrometry (SIMS) analyses detected trace gold in the coarse, near-stoichiometric pyrite in overprinted samples. The pregold vein assemblage was fractured and cemented by gold ore-stage mineralization

The gold ore-stage assemblage consists of gold- and arsenic-enriched pyrite and marcasite encompassed by jasperoid and drusy quartz, and local late fluorite, orpiment, and galkhaite. The consistent spatial association of jasperoid and ore pyrite reflects their near-contemporaneous formation. The ore pyrite occurs as either fine, irregularly shaped grains, or rims on earlier, gold-free pyrite. In thin section, the pyrite is visibly distinct and has a low polishing relief and a poor polish. SIMS and electron microprobe analyses show that ore pyrites commonly contain 8 to 11 wt percent arsenic and as much as 2,400 ppm gold. Near the end of the ore stage, fluorite, orpiment, and galkhaite precipitated locally in open space created by faulting or limestone dissolution.

Late ore-stage mineralization consists dominantly of open space-filling realgar and calcite, with minor quartz, stibnite, and framboidal pyrite. Realgar conforms to euhedral crystal faces of ore-stage quartz, fluorite, and galkhaite. Calcite filled most remaining open space and conforms to euhedral crystal faces of quartz, fluorite, and realgar.

Significant textural observations argue against an earlier interpretation that the gold mineralization and arsenic minerals formed as two discrete events separated by 40 m.y. In a few areas where calcite and realgar are in contact with ore-stage quartz containing gold-bearing pyrite, realgar and calcite enclose gold-bearing pyrite grains. Massive realgar and calcite distal from these contacts do not contain the gold-bearing pyrite. The presence of ore pyrite in realgar, calcite, and jasperoid requires close timing of these minerals and shows that there is no major time break separating ore-stage and late ore-stage mineral deposition. Textures indicate, instead, that the ore stage and late ore stage formed as part of a single, evolving hydrothermal system. The consistent successive overgrowth of younger minerals on perfectly preserved euhedral faces of older minerals supports the continuous evolution of the gold ore stage into the late ore stage. These results are consistent with fluid inclusions that indicate that paragenetically successive minerals precipitated from an aqueous ore fluid with consistent salinity and gas contents but at declining temperatures. Results show that, within error, the 34, 39, and 42 Ma ages determined for fluorite and galkhaite at Getchell and adularia at the nearby Twin Creeks mine, respectively, most closely approximate the timing of gold deposition at Getchell.

Introduction

More than 11 percent of the current world's gold production is supplied by the state of Nevada (Nevada Bureau of Mines and Geology, 1999), and most of this gold is mined from Carlin-type gold deposits These deposits were first recognized as a new class of deposit following the discovery of Carlin in the mid 1960s. Since then, more than 1,000 t of gold has been produced (Christensen, 1995) from more than 100 Carlin-type gold deposits in Nevada. In spite of this activity, there is no widely accepted genetic model for these systems. It has been difficult to relate gold precipitation to specific geologic events and processes because the submicron size of the gold and fine-grained ore and gangue minerals have made it hard to determine the ore paragenesis, generally no minerals in the gold ore assemblage are amenable to radiometric dating, and deposit temperatures are sufficiently low so as not to thermally perturb K-bearing phases in the country rocks (Folger et al., 1996; Hofstra et al., 1999). As a result, geologic processes responsible for transporting and precipitating gold have not been consistently identified. This study seeks to clarify questions concerning the sequence of mineral precipitation and the timing of gold and arsenic sulfide mineral precipitation at the Getchell deposit.

In previous studies of Carlin-type gold deposits, gold was observed to be spatially associated with pyrite (Hausen and Kerr, 1968; Wells and Mullens, 1973; Radtke, 1985; Bakken, et al., 1989; Chryssoulis, 1990; Arehart et al., 1993a), quartz (Bakken et al., 1989), clay minerals (Hausen and Kerr, 1968; Bakken et al., 1989), and cinnabar and realgar (Bakken et al., 1989). Recent studies using secondary ion mass spectrometry (SIMS) show that submicron gold is present in arsenic-rich zones in pyrite and marcasite at the Post-Betze, Gold Quarry, Chimney Creek (Arehart et al., 1993a; Simon, et al., 1999), and Meikle (Lamb, 1995) deposits.

[†] E-mail, jcline@nevada.edu

The association of gold with arsenic sulfide minerals is a well-known characteristic of Carlin-type gold deposits (Arehart, 1996); however, gold and arsenic minerals generally did not precipitate together. Paragenetic studies at Mercur (Jewell and Parry, 1987), Jerritt Canyon (Hofstra et al., 1991), Post-Betze (Arehart et al., 1993b), Carlin (Bakken and Einaudi, 1986; Kuehn and Rose, 1995), and Twin Creeks (Stenger et al., 1998; Simon et al., 1999) indicate that precipitation of gold and gold-bearing pyrite typically preceded precipitation of realgar and orpiment.

The age of Carlin-type gold deposition has been a contentious issue, and a wide range of ages from Jurassic to Tertiary has been reported. The oldest ages for some deposits have been obtained from sericite and illite interpreted to be genetically associated with gold. These ages range from ~150 Ma at Mercur, Utah (Wilson and Parry, 1995) to ~117 Ma at Post-Betze (Arehart et al., 1993c), ~95 Ma at Genesis and Blue Star (Drewes-Armitage et al., 1996), and 90 to 83 Ma at Getchell (Silberman et al., 1974; Groff et al., 1997). These ages may be much older than the gold deposits as they are generally from incompletely reset preore micas or from mixtures of preore and ore-stage mica (Folger et al., 1996; Hofstra et al., 1999). Crosscutting relationships between gold mineralization and dated igneous rocks suggest that at least some gold mineralization is Tertiary in age. For example, mineralization is younger than a 37.3 Ma rhyolite dike at the Beast deposit (Ressel et al., 1998, 2000), a 40.8 Ma basalt dike at Jerritt Canyon (Hofstra, 1994; Hofstra et al., 1999), and a 39.3 Ma biotite-feldspar porphyry dike (Arehart et al., 1993c) at the Betze-Post deposit (Emsbo et al., 1996). Following a rigorous evaluation of ages available for Jerritt Canyon and other Carlin-type gold deposits, Hofstra et al. (1999) concluded that the most reliable ages constrain mineralization to the mid-Tertiary, between 42 and 30 Ma.

The Getchell deposit in north-central Nevada (Fig. 1) is a typical Carlin-type gold deposit; however, the main stage of gold mineralization has been determined to be about 40 m.y. older than spatially associated arsenic minerals (Groff et al., 1997). The earliest paragenetic study of this deposit was conducted by Joralemon (1951), who reported that early sulfide minerals, including pyrite, arsenopyrite, chalcopyrite, and pyrrhotite, were followed by late orpiment, realgar, and marcasite. Sparse, visible disseminated gold particles were observed on both early and late sulfide minerals, but early porous pyrite was coincident with the richest ore. Joralemon (1951) concluded that submicroscopic gold had precipitated with the late minerals but that most gold had precipitated on the early porous pyrite. Gold mineralization was interpreted to have accompanied Tertiary volcanism.

Silberman et al. (1974) used conventional K-Ar methods to date igneous rocks and sericite spatially associated with gold at Getchell. They interpreted that emplacement of a granodiorite stock and related andesite porphyry dikes, sericite alteration, and gold mineralization were all part of a magmatic-hydrothermal event that occurred approximately 90 Ma.

In a recent study at Getchell and the nearby Twin Creeks deposit, Groff et al. (1997) concluded that approximately 40 m.y. elapsed between the main stage of gold mineralization and deposition of the arsenic sulfide mineral assemblage. They described five stages of mineralization, several of which they dated using $^{40}Ar/^{39}Ar$ step-heating techniques. Stages 1 and 2 formed at 95 and 92 Ma and include pyrrhotite skarn and garnet skarn, and base metal vein mineralization, respectively, related to emplacement of the Osgood granodiorite

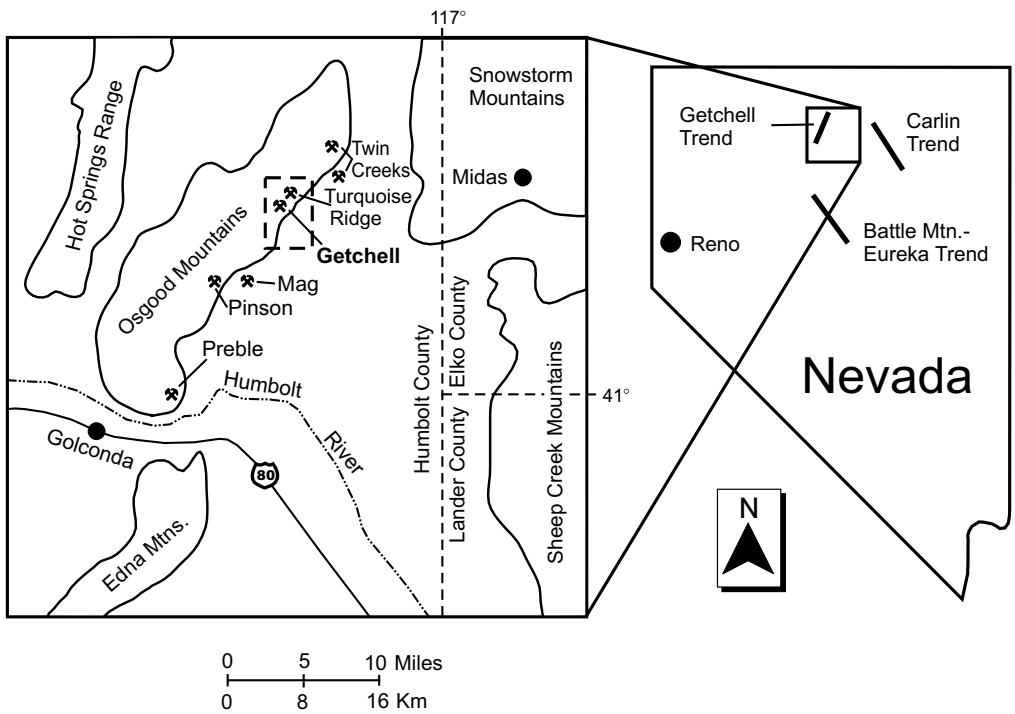

FIG. 1. Location of the Getchell deposit and other mines in the Getchell Trend (modified from Pitkin, 1991). Dashed box shows location of Figure 2.

stock and related dikes. Stage 4 consists of 75 Ma low-grade gold mineralization in a breccia pipe. Stages 3 and 5 are described as Carlin-type mineralization and both stages exhibit multiple fracturing and mineral precipitation events. Stage 3, at ~ 83 Ma, is the major gold event and comprises quartz, pyrite, arsenopyrite, kaolinite, K feldspar, sericite, and gold. Visible gold was not observed and its location was not determined, but gold is described as closely associated with pyrite-rich quartz in the matrix of breccias. Two samples of sericite in chlorite from a dacite dike and the Osgood granodiorite stock, collected from the North and Main pits, respectively, and a third sample of secondary K feldspar from a granodiorite plug located 3 km east of the Main pit, gave ages ranging from 81.2 to 84.3 Ma. Stage 5 mineralization forms a matrix for stage 3 clasts, an open-space assemblage in structures, and veins crosscutting stage 3. The assemblage contains realgar, quartz, pyrite, stibnite, orpiment, gold, and calcite. Gold was not observed but based on assay information, seemed to be most closely associated with orpiment and pyrite. The assemblage is interpreted to have formed at 42 Ma, approximately 40 m.y. after the main gold event, based on dating of adularia from an assemblage similar to stage 5 at the nearby Twin Creeks deposit.

The current study was conducted to examine the temporal relationships between gold and gangue minerals, including arsenian pyrite, quartz, fluorite, and arsenic sulfide minerals at Getchell. Gangue minerals reflect both replacement and precipitation in open space, in and adjacent to the Getchell fault zone. This mineralization displays significant crosscutting and overgrowth textures not observed in most Carlin-type gold deposits. Ion probe and electron microprobe techniques were used to locate and quantify gold mineralization and were combined with petrography to identify ore-stage, preore, and postore minerals. The results of this study are used to constrain the timing of gold deposition at Getchell.

Geology

The Getchell deposit is located in the northern Osgood Mountains in north-central Nevada, in a region of complexly folded and faulted Paleozoic sedimentary rocks (Fig. 2). This

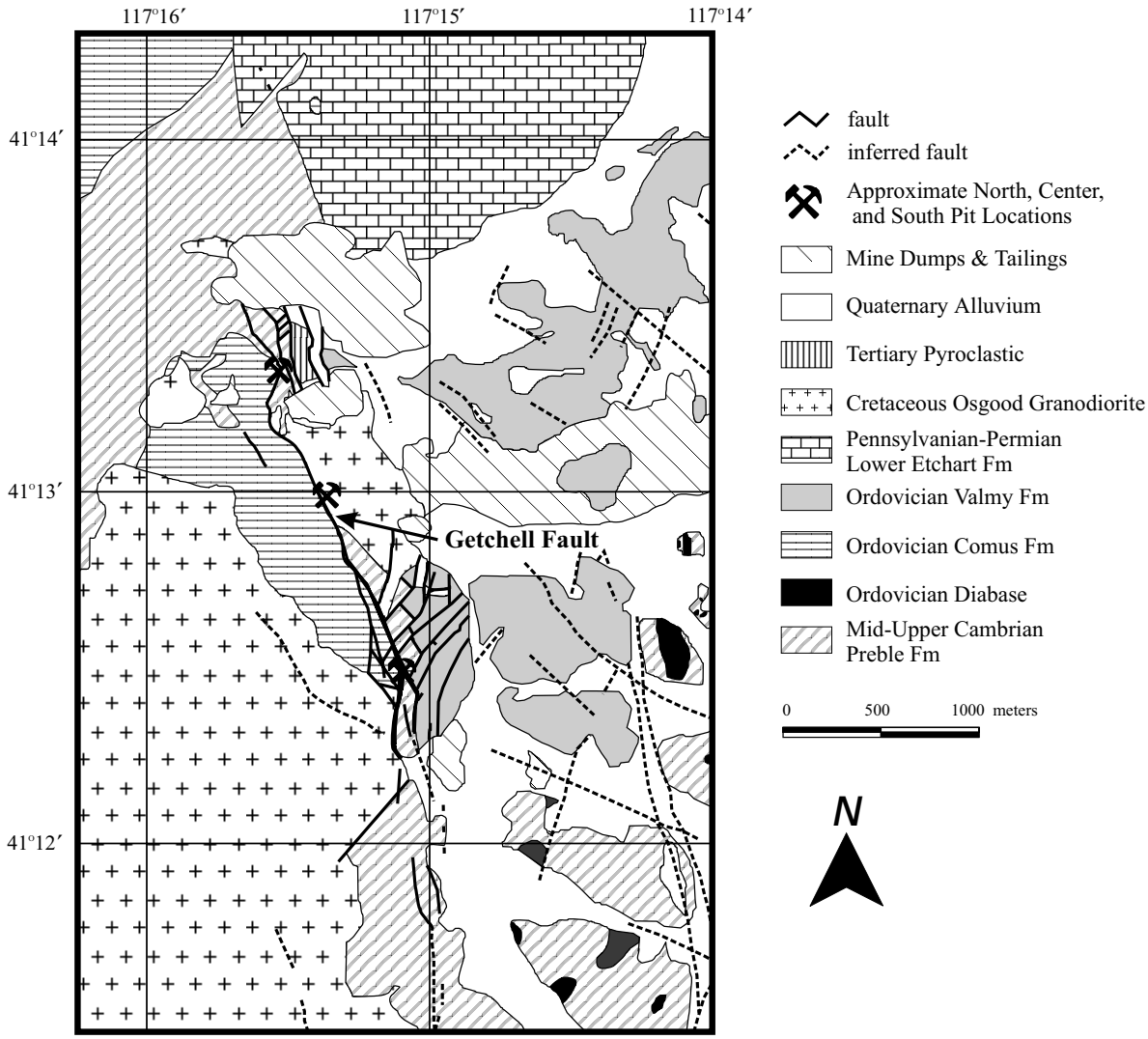

FIG. 2. Geology of the Getchell gold deposit. Approximate North, Center, and South pit locations are indicated by mine symbols (modified from an unpublished map provided by M. Gingrich, Getchell Gold, Inc., 1998).

part of Nevada coincided with the western margin of the North American craton during the early Paleozoic. To the east, an early Paleozoic shallow-water, continental-shelf carbonate facies of limestone and dolomite with minor shale and sandstone was deposited. An assemblage of offshore, deep-water siliceous chert, shale, quartzite, and mafic volcanic rocks interbedded with thin calcareous units was deposited to the west (Stewart, 1980). Three contractional orogenies juxtaposed these sedimentary units. Thrusting of western assemblage rocks over eastern assemblage rocks during the Late Devonian and Early Mississippian Antler orogeny formed the Roberts Mountain thrust fault (Hotz and Willden, 1964; Stewart, 1980). Post-Antler siliciclastic rocks were transported eastward over the Roberts Mountain allochthon during the Late Permian and Early Triassic Sonoma orogeny (Silberling and Roberts, 1962; Stewart, 1980). Thrust faults developed near the old Paleozoic shelf-slope hinge line during the Middle Jurassic as part of the Luning-Fencemaker belt (Oldow, 1984; Burchfiel et al., 1992) and during the Late Cretaceous Sevier orogeny (Armstrong, 1968). Windows developed in the upper plate of the Roberts Mountain thrust fault during subsequent uplift, extension, and erosion (Hotz and Willden, 1964; Stewart, 1980). Locally, exposed carbonate rocks of the lower plate of the Roberts Mountains thrust host the Getchell deposit and most other Carlin systems.

Gold mineralization at Getchell occurs in the Cambrian Preble and Ordovician Comus Formations within and adjacent to the north-northwest-trending, steeply dipping Getchell fault system. The Osgood granodiorite stock and related andesite dikes intruded the Paleozoic sedimentary rocks approximately 92 to 90 Ma (Silberman et al., 1974; Groff et al., 1997) and created a wide contact metamorphic aureole containing localized scheelite and molybdenite mineralization (Hotz and Willden, 1964). Phylitic shale in the mid-upper parts of the Preble Formation near the deposit has been contact metamorphosed to biotite hornfels (M. Gingrich, J. Culver, pers. commun., 1998). The unit crops out in the hanging wall of the Getchell fault near the North and South pits (Fig. 2; M. Gingrich, pers. commun., 1998). The Comus Formation, originally limestone and shale, was metamorphosed to black, carbonaceous hornfels; a large block forms the footwall of the Getchell fault zone in all three pits (Fig. 2; M. Gingrich, pers. commun., 1998). The Valmy Formation was probably thrust from the west during the Antler orogeny. The unit contains chert, siliceous shales, quartzite, and volcanic rocks (Hotz and Willden, 1964) and crops out in the hanging wall of the South pit.

The Getchell fault zone trends N 10° to 15° W in the vicinity of the Getchell deposit (Nanna et al., 1987) and cuts Paleozoic sedimentary rocks and the northeast flank of the granodiorite stock (Fig. 2). The fault zone consists of anastomosing strands that coalesce at depth (Joralemon, 1951) and dip 40° to 75° NE (Nanna et al., 1987). The age of faulting is poorly constrained, but multiple periods of movement are indicated. Andesite dikes follow the trend of the fault zone or occupy it, indicating that fracture zones existed prior to 90 Ma. Highly sheared andesite dikes in the North pit document postintrusion movement. Postmineral movement is indicated by the development of slickensides on the surfaces of altered rock and displacement of Quaternary alluvium (Silberman et al., 1974). Horizontal mullions and slickensides show that fault movement was largely parallel to strike (Hobbs, 1948). Superimposed, vertical slickensides indicate that dip-slip movement occurred subsequent to strike-slip movement (Joralemon, 1951).

Recent fluid inclusion studies (Groff, 1996; Cline and Hofstra, 2000) have provided information about fluids related to quartz and base metal vein mineralization, which is probably associated with the granodiorite intrusion and gangue minerals associated with gold. Inclusions associated with quartz and base metal vein mineralization have a wide range of homogenization temperatures, 120° to > 300°C, and inclusion fluids have variable and gas-rich compositions and contain abundant CO_2, CH_4, and lesser N_2 (Cline and Hofstra, 2000).

Inclusions in gangue minerals associated with gold are distinctly different from inclusions in earlier vein quartz. Gold-bearing jasperoid and drusy quartz precipitated over a temperature range of 180° to 240°C from an aqueous fluid with a salinity of about 4 to 6 wt percent NaCl equiv (Cline and Hofstra, 2000). Other gangue minerals precipitated at lower temperatures. Primary inclusions in fluorite were trapped at about 175°C; most secondary inclusions were trapped in fluorite and calcite at 115° to 155°C (Cline and Hofstra, 2000). Salinities of inclusions in fluorite and calcite are consistently 4 to 5 wt percent NaCl equiv. Homogenization temperatures of most fluid inclusions in orpiment ranged from 120° to 180°C (Groff, 1996). Applying the same pressure correction used above (Cline and Hofstra, 2000), trapping temperatures were approximately 135° to 200°C. Salinities of most inclusions in orpiment varied from 4 to 6 wt percent NaCl equiv, but a few salinities as high as 12 to 14 wt percent were recorded (Groff, 1996). Quadrupole mass spectrometer analyses of inclusion fluids in quartz and calcite (Cline and Hofstra, 2000) and orpiment (Groff, 1996) indicate ore fluids were dominantly aqueous but contained approximately 2 to 4 mole percent CO_2, minor CH_4, and trace H_2S (Hofstra and Cline, 2000). As the gases contribute to the freezing point depression, the actual salinity of the fluid is probably about 2 to 4 wt percent NaCl equiv (Hofstra and Cline, 2000).

Methods

Approximately 450 samples were collected from ore and waste in the North, Center, and South pits (Fig. 3), core holes drilled in and adjacent to the three open pits (Fig. 3), altered and veined granodiorite west of the pits, skarn deposits located at the contacts of the granodiorite and sedimentary rocks, and selected ore horizons in the Northwest ore zone of the Getchell underground mine. Most samples were collected from surface outcrops in or near the open pits. Samples were collected from all lithologies and mineralization and alteration assemblages. Sample transects into and out of ore zones were collected from drill core. Duplicate samples, other than drill core, were collected from most sites and were analyzed for gold by fire assay.

Polished sections for transmitted and reflected light petrography and electron and ion microprobe studies were prepared from about 200 samples selected on the basis of hand specimen petrography, assays, and mapping of sample traverses. Selected samples exhibited overgrowth and crosscutting textures and ranged from barren waste to ore containing greater than 30 g/t gold. Ion microprobe and electron microprobe

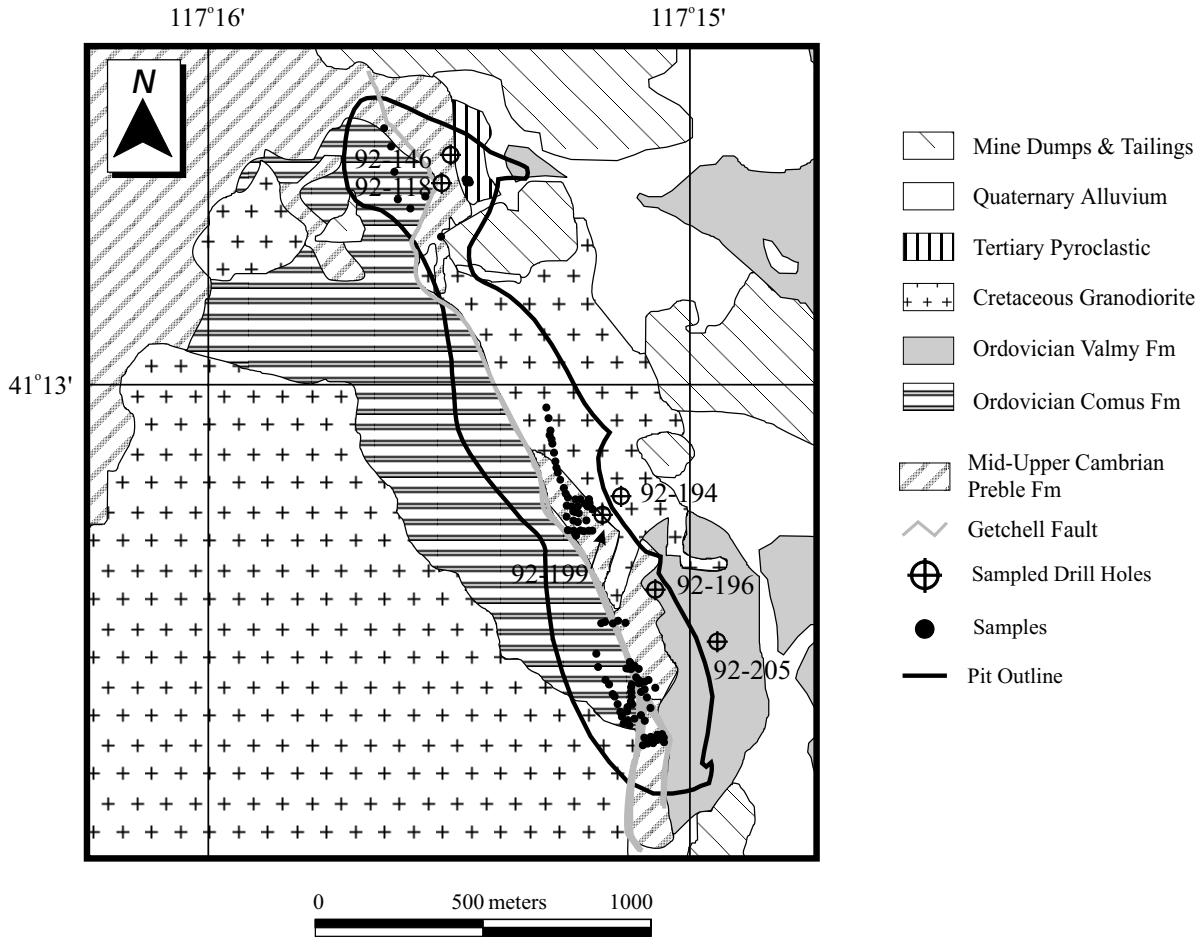

FIG. 3. Map showing surface sample locations, locations of sampled drill holes, and approximate outline of the North, Center, and South pits.

analyses were used to locate and quantify gold and arsenic in pyrite and marcasite and formed the basis for the paragenetic study. Some of the fine, gold-bearing iron sulfide grains can be identified as marcasite rather than pyrite. Most, however, are too fine, or too poorly polished to make this determination and are referred to as iron sulfide minerals. After gold-bearing iron sulfide minerals were identified, crosscutting and growth relationships permitted ore-stage and pre- and postgold assemblages to be identified.

Integrated SIMS and electron microprobe analyses (EMPA) were used to locate and quantify gold. SIMS analyses were obtained using a CAMECA model IMS-3f ion microprobe at the University of Western Ontario. The ion probe provides quantitative gold analyses with low detection limits (0.32 ppm; Chryssoulis, pers. commun., 1995), but the spot size (30-μm diam) is large relative to the size of the analyzed pyrite grains. Elba pyrite with implanted gold was used for standardization (Chryssoulis et al., 1987). EMPA have significantly higher detection limits (Table 1) than the ion probe, but the small analyzed spot size (~2-μm diam) minimizes analysis of material adjacent to the grain of interest. EMPA for iron, sulfur, and trace metals were obtained using Cameca SX-50 electron microprobes at Virginia Polytechnic Institute and State University and the University of Arizona and using a JOEL JXA733 microprobe at the University of New Mexico. Analyses at Virginia Polytechnic Institute and State University and the University of Arizona quantified Fe, S, and As in pyrites in five samples and were collected at 15 kV with a beam current of 20 nA. X-ray maps were produced at 30 kV with a beam current of 600 nA (Virginia Polytechnic Institute and State University). Standards included troilite and GaAs (University of Arizona) and two pyrites containing trace As (Virginia Polytechnic Institute and State University). Ten samples were analyzed at the University of New Mexico for a larger suite of trace metals, including gold, at 25kV using a 50 nA beam current. Natural pyrite, galena, cinnabar, and sphalerite were used to standardize Fe, S, Pb, Ag, Hg, and Zn. Pure elements were used to standardize Co, Ni, Cu, Au, and Mo. Synthetic GaAs, TlCl, and Sb_2Te_3 were used to standardize As, Tl, and Sb and Te, respectively.

Mineral Paragenesis

Integrated petrography, SIMS, and EMPA show that multiple discrete hydrothermal events occurred in the vicinity of the Getchell deposit. Temporally related gold ore and late

TABLE 1. Electron Microprobe Analyses of Pyrite and Marcasite Grains (Au and Ag in ppm, all other values in wt %)

Detection limit (1σ)	Sample	Fe	S	Co 0.010	Ni 0.011	Pb 0.070	Zn 0.012	Mo 0.066	Te 0.030	Ag 800	As 0.030	Au[1] 140* 400**	Cu 0.015	Sb 0.035	Hg 0.050	Tl 0.060	Total
Preore pyrite	G6-30-85	45.53	53.61	0.032	bdl	NA	bdl	NA	NA	bdl	0.212	bdl**	0.022	0.288	0.084	bdl	100.46
		45.75	53.78	0.032	bdl	NA	bdl	NA	NA	bdl	0.058	bdl**	bdl	0.038	bdl	bdl	100.17
		46.05	54.27	0.045	bdl	bdl	bdl	NA	NA	bdl	0.072	bdl**	bdl	bdl	bdl	bdl	100.43
		45.79	53.24	0.053	bdl	bdl	bdl	NA	NA	bdl	0.112	bdl**	bdl	bdl	bdl	bdl	99.19
	92-205 1079	45.48	53.69	0.055	bdl	bdl	bdl	NA	NA	bdl	bdl	bdl**	bdl	bdl	bdl	bdl	99.23
		46.04	53.77	0.059	bdl	bdl	bdl	NA	NA	bdl	bdl	bdl**	bdl	bdl	bdl	bdl	99.87
		45.23	53.97	0.055	bdl	bdl	bdl	NA	NA	bdl	bdl	bdl**	bdl	bdl	bdl	bdl	99.26
		45.03	52.62	0.068	bdl	bdl	bdl	NA	NA	bdl	bdl	bdl**	bdl	bdl	bdl	bdl	97.71
		44.66	53.30	0.203	0.297	bdl	bdl	NA	NA	bdl	0.167	bdl**	bdl	bdl	bdl	bdl	98.63
	G6-23-27	43.54	53.62	bdl	bdl	0.398	bdl	NA	NA	4488	2.898	bdl**	bdl	0.031	bdl	bdl	100.90
		45.22	50.98	bdl	bdl	bdl	bdl	NA	NA	bdl	1.602	bdl**	bdl	0.392	bdl	bdl	98.20
	G6-22-8	46.08	53.78	bdl	bdl	bdl	bdl	NA	NA	bdl	bdl	bdl**	bdl	bdl	bdl	bdl	99.86
		46.17	53.32	bdl	bdl	bdl	bdl	NA	NA	bdl	bdl	bdl**	bdl	bdl	bdl	bdl	99.48
		46.33	53.45	bdl	bdl	bdl	bdl	NA	NA	bdl	bdl	bdl**	bdl	bdl	bdl	bdl	99.78
		45.90	52.68	0.039	bdl	bdl	bdl	NA	NA	bdl	1.266	bdl**	bdl	bdl	bdl	bdl	99.89
		46.22	52.36	bdl	bdl	bdl	bdl	NA	NA	bdl	0.311	bdl**	bdl	bdl	bdl	bdl	99.89
		45.89	53.02	bdl	bdl	bdl	bdl	NA	NA	bdl	0.255	bdl**	bdl	bdl	bdl	bdl	99.16
		45.73	52.53	bdl	bdl	bdl	bdl	NA	NA	bdl	0.857	bdl**	bdl	bdl	bdl	bdl	99.12
	92-118 59.5	46.82	53.79	0.048	bdl	0.215	bdl	bdl	bdl	bdl	0.281	bdl*	bdl	bdl	bdl	0.133	101.29
		46.55	52.75	0.037	bdl	0.209	0.014	bdl	bdl	bdl	0.285	bdl*	0.115	0.102	bdl	0.091	100.15
Ore pyrite-marcasite	G6-30-85	42.26	48.96	0.064	0.018	bdl	0.014	NA	NA	bdl	7.440	1450**	0.093	0.087	0.314	0.531	99.90
		42.56	47.62	0.055	0.016	bdl	bdl	NA	NA	bdl	8.125	1510**	0.089	0.100	0.321	0.631	99.65
	92-205 1079	41.85	53.17	0.065	0.019	bdl	bdl	NA	NA	bdl	5.282	2380**	0.135	0.045	0.040	bdl	100.74
	G93F3-O	44.64	51.44	0.030	0.127	bdl	bdl	NA	NA	bdl	3.524	540**	0.233	0.284	0.099	0.308	100.58
		44.32	50.48	0.035	bdl	bdl	bdl	NA	NA	bdl	3.369	bdl**	0.241	0.238	bdl	0.150	98.83
		43.94	50.63	0.024	0.014	bdl	bdl	NA	NA	bdl	3.123	bdl**	0.247	0.207	bdl	0.095	98.16
	92-118 59.5	43.38	45.69	0.059	bdl	0.178	0.023	bdl	0.172	bdl	10.491	400*	0.117	bdl	0.130	0.357	100.70
	92-118 68	41.96	47.01	0.051	0.022	0.215	bdl	bdl	0.031	bdl	10.946	190*	0.561	bdl	bdl	bdl	100.74
		41.10	45.74	0.036	bdl	0.193	bdl	bdl	0.050	bdl	10.847	310*	0.663	bdl	bdl	0.075	98.61
		41.97	46.38	0.049	bdl	0.206	bdl	bdl	bdl	bdl	10.093	bdl*	0.578	bdl	bdl	bdl	99.28
		41.57	45.94	0.046	bdl	0.223	bdl	bdl	bdl	bdl	9.926	190*	0.518	bdl	bdl	0.342	98.57
		41.56	47.32	0.043	bdl	0.210	bdl	bdl	0.061	bdl	8.114	280*	0.370	bdl	bdl	0.288	97.99
		41.38	47.06	0.030	0.023	0.132	bdl	bdl	bdl	bdl	10.799	200*	0.319	bdl	bdl	bdl	99.74
		40.92	46.62	0.049	bdl	0.130	bdl	bdl	bdl	bdl	10.510	710*	1.074	bdl	bdl	bdl	99.38
		41.88	49.47	0.037	bdl	0.220	0.017	bdl	bdl	bdl	5.940	480*	0.356	0.036	bdl	0.090	97.95
		41.18	46.56	0.051	0.015	0.164	bdl	bdl	bdl	bdl	10.531	220*	0.824	bdl	bdl	bdl	99.32
		34.38	45.35	0.066	0.023	0.181	0.035	bdl	0.112	bdl	11.270	1870*	0.745	1.709	1.268	2.775	98.07
		41.79	47.02	0.050	bdl	0.175	0.014	bdl	bdl	bdl	8.894	bdl*	0.518	bdl	bdl	bdl	98.45
		41.60	48.63	0.044	bdl	0.218	0.014	bdl	bdl	bdl	6.812	660*	0.426	0.230	bdl	0.600	98.63
		41.41	48.19	0.050	bdl	0.140	bdl	bdl	bdl	bdl	7.446	740*	0.414	0.727	bdl	0.234	98.03
		40.86	45.40	0.058	bdl	0.214	0.029	bdl	bdl	bdl	10.675	bdl*	0.700	bdl	bdl	bdl	97.94
		41.33	47.09	0.062	bdl	0.165	0.008	bdl	bdl	bdl	8.785	460*	0.519	bdl	bdl	0.774	98.01
Hydrothermal(?) Coarse marcasite	GQR2	46.46	52.81	0.097	0.018	bdl	bdl	NA	NA	bdl	0.054	bdl**	bdl	0.033	bdl	bdl	99.43
		45.80	52.26	0.093	0.027	bdl	bdl	NA	NA	bdl	0.265	bdl**	0.027	0.073	bdl	bdl	98.54
		46.35	53.08	0.197	0.049	bdl	bdl	NA	NA	bdl	0.065	bdl**	0.025	0.080	bdl	0.085	99.85
		45.93	53.20	0.094	0.035	bdl	bdl	NA	NA	bdl	0.089	bdl**	0.018	0.100	bdl	bdl	99.44
		45.88	53.31	0.101	0.034	bdl	bdl	NA	NA	bdl	0.056	bdl**	0.273	0.077	bdl	0.061	99.73
		45.62	53.80	0.147	0.034	bdl	bdl	NA	NA	bdl	0.056	bdl**	0.407	bdl	bdl	bdl	100.07

TABLE 1. *(Cont.)*

Detection limit (1σ)	Sample	Fe	S	Co 0.010	Ni 0.011	Pb 0.070	Zn 0.012	Mo 0.066	Te 0.030	Ag 800	As 0.030	Au[1] 140* 400**	Cu 0.015	Sb 0.035	Hg 0.050	Tl 0.060	Total
Au-bearing marcasite	G7-15-13	45.71	52.63	0.054	0.057	bdl	bdl	NA	NA	bdl	1.846	bdl**	bdl	bdl	bdl	bdl	100.30
		44.37	52.77	0.045	bdl	bdl	0.015	NA	NA	bdl	2.774	720**	0.047	0.065	bdl	0.076	100.07
		44.53	50.86	0.072	0.084	bdl	bdl	NA	NA	bdl	3.644	730**	0.031	bdl	0.084	0.087	99.23
		44.01	51.88	0.044	0.025	bdl	bdl	NA	NA	bdl	4.369	660**	0.034	bdl	0.071	0.084	100.63
		44.12	51.04	0.035	bdl	bdl	0.023	NA	NA	bdl	2.696	880**	0.027	0.065	bdl	bdl	98.01
Late ore framboids	GQR-4	45.34	51.55	0.036	bdl	0.214	bdl	bdl	bdl	1130	1.777	bdl*	0.019	bdl	bdl	bdl	99.05
		44.47	51.49	0.047	bdl	0.288	bdl	bdl	0.033	2660	bdl	220*	bdl	bdl	bdl	1.934	98.56

Abbreviations: bdl = below detection limit, NA = not analyzed

[1] Gold has two detection limits; measurements were made in two sessions evaluating different peaks, and counting statistics determined different standard deviations for the two sets of analyses Au analyses for analyzed samples: G6-30-85 = 7.7 g/mt (0.248 oz/t); 92-205 1079 = 7.0 g/mt (0.226 oz/t); G6-23-27 = 7.8-15.6 g/mt (0.25-0.50 oz/t); G6-28-8 = 0.5 g/mt (0.016 oz/t); 92-118 59.5 = 30.8 g/mt (0.992 oz/t); GQR2 = 7.8 to 15.6 g/mt (0.25-0.50 oz/t); G93F3-O was not assayed; 92-118 68 = 19.7 g/mt (0.634 oz/t); G7-15-13 = 9.3 g/mt (0.300 oz/t); GQR4 = 7.8 to 15.6 g/mt (0.25-0.50 oz/t)

gold ore stages (Fig. 4) were also identified during these studies. Pregold quartz veins containing minor pyrite are commonly fractured and locally cemented by later gold ore-stage minerals. Gold occurs in fine-grained, arsenic-enriched pyrite associated with jasperoid and minor orpiment, fluorite, and galkhaite. Gold deposition was followed by a gold-poor or gold-free, but arsenic-enriched, late ore stage. Micas were not present in most ore samples from the open pits and, where identified, were associated with quartz veins in the granodiorite. Minor translucent, euhedral calcite precipitated, probably after the gold-bearing hydrothermal event.

Preore mineralization

Preore quartz veins, containing minor disseminated pyrite and trace sphalerite, chalcopyrite, galena, and arsenopyrite (Fig. 4), crosscut sedimentary rocks, cement brecciated granodiorite, and are spatially associated with the northeast perimeter of the Osgood stock. Gold was not observed and analyses indicate that veins contain nil to very low gold. Milky white vein quartz is typically coarse, anhedral, fractured, and commonly exhibits undulatory extinction. Trails of abundant, small, secondary fluid inclusions give the quartz a wispy appearance in thin section and the milky white color observed in hand specimen. Both vein quartz and pyrite are commonly fractured and locally cemented by ore- and late ore-stage minerals. Minor, fine-grained white mica, probably sericite, occurs in granodiorite near quartz veins or along vein selvages. Clays and micas, observed in a only few samples collected from the open pits, are more abundant in the Getchell Underground deposit, probably reflecting an increased abundance of igneous rocks at depth (Cail, 1999; K. Weaver, pers. commun., 1999). Remnant calcite masses in some veins are small, medium gray, mottled, and fine to medium grained and are most likely remnants of limestone or early calcite mineralization.

Pyrite disseminated in the milky quartz veins is relatively coarse, anhedral to euhedral, and, in thin section, exhibits high relief and a smooth polish (Fig. 5A). Ion probe analyses of 6 grains (Table 2, analyses 1–6) indicate that gold concentrations vary from 0.55 to 17 ppm (mean = 6.1 ppm); arsenic varies from 0.18 to 1.1 wt percent (mean = 0.45 wt %). The analyzed spot size is large and detected gold may reside in gold-bearing, ore-stage pyrite grains included in the analysis. The correlation between low gold and arsenic in pyrite determined by SIMS is illustrated in Figure 6.

These quartz plus minor pyrite veins are clearly pregold ore, as both quartz and pyrite are commonly fractured and locally cemented by ore-stage minerals, including quartz, realgar, and gold- and arsenic-enriched pyrite. At least some of the coarse pyrite forms gold-free pyrite cores on which gold-bearing iron sulfide minerals were deposited (Fig. 5B). EMPA of these pyrites show near-stoichiometric concentrations of iron and sulfur (Table 1). The pyrites generally contain <1.0 wt percent arsenic; however, as much as 3 wt percent may be present. Gold in all EMPA was below the detection limit (Table 1). As a result, in a plot of gold versus arsenic (Fig. 6), these gold-poor pyrites plot at the origin or at low arsenic values and nil gold. Pyrite cores are free of most other trace elements, but ~0.05 wt percent cobalt, a common substitute for iron, is typically present. EMPA analyses are consistent with SIMS analyses.

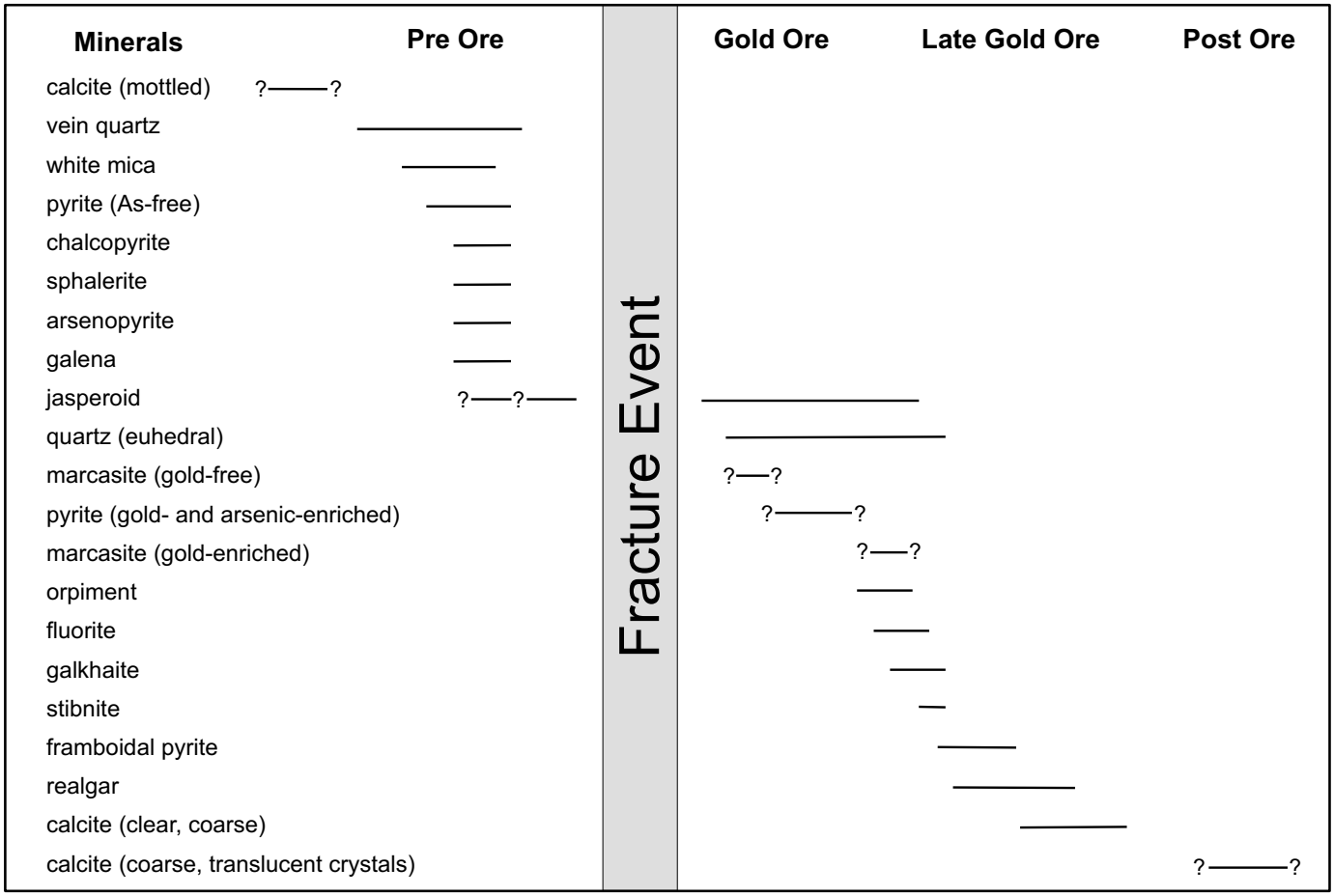

FIG. 4. Paragenesis of minerals in preore, gold ore, late gold ore, and postore stages.

Fluid inclusion characteristics determined by Groff (1996) for his stage 3 quartz associated with major gold mineralization are very similar to fluid inclusion characteristics determined by Cline and Hofstra (2000) for preore vein quartz. Characteristics identified in both studies include the presence of liquid- and vapor-rich aqueous inclusions, homogenization to liquid at temperatures ranging from 100° to >300°C, with most inclusions homogenizing between ~150° and 230°C, salinities of 0 to about 20 wt percent NaCl equiv, with most salinities between 3 and 9 wt percent, decrepitation of some inclusions prior to liquid-vapor homogenization at temperatures of 200° to >300°C, the presence of three-phase inclusions with small, translucent daughter crystals, probably calcite, that did not melt during heating, the presence of abundant but variable CO_2 and CH_4 identified during microthermometry and by quadruple mass spectrometer gas analyses, and the presence of lesser N_2, identified by quadruple mass spectrometer analyses. These observations suggest that the stage 3 quartz of Groff (1996) may be the same as, or similar to the preore vein quartz described above. At the very least, stage 3 quartz is quite different from jasperoid that contains a single population of two-phase aqueous inclusions (Cline and Hofstra, 2000) and which was determined by SIMS and EMPA, described below, to be the primary host for gold at Getchell. As a result, it appears unlikely that sericite and adularia associated with stage 3 quartz and dated at ~83 Ma are temporally associated with gold mineralization.

In summary, trace to nil gold is present in coarse pyrite that is associated with pregold, hydrothermal veining. These pyrites contain minor to nil arsenic and generally lack other trace metals. Vein quartz and pyrite are commonly fractured and locally cemented by gold ore-stage minerals, and some of these pyrite crystals probably form the barren cores on which gold- and arsenic-enriched pyrite precipitated. This assemblage is spatially associated with the perimeter of the Osgood stock and may be related to intrusion of the granodiorite.

Gold ore mineralization

The gold ore-stage assemblage consists of gold-bearing arsenian pyrite and marcasite enclosed by jasperoid; minor orpiment, fluorite, and rare galkhaite precipitated locally in open space near the end of the gold ore stage (Fig. 4). Gold-bearing pyrite and marcasite typically formed anhedral grains, commonly less than 4 μm in diameter. In thin section they have a fuzzy rim, low polishing relief, and a poor polish (Fig. 5B). Less commonly, gold-bearing iron sulfides form rims around gold-free pyrite cores (Fig. 5B). These rims have the same characteristics as the anhedral grains and are generally <2 μm thick. In higher grade ore, grains and rims are coarser and more abundant.

TABLE 2. Secondary Ion Mass Spectrometry (SIMS) Analyses of Fine- and Coarse-Grained Pyrite and Marcasite

Analysis no.	Sample no.[1]	Au (ppm)	As (wt%)	Description
1	G6-25-47	11	0.33	Coarse euhedral marcasite rimming fine-grained marcasite
2	G6-25-47	5.2	0.40	Coarse pyrite without visible rim or fractures
3	G7-16-14	17	1.10	Center of coarse pyrite with microcrystalline pyrite rim
4	G7-16-14	0.72	0.21	Coarse pyrite with no visible rim
5	G7-16-14	0.55	0.49	Coarse pyrite with no visible rim
6	G7-16-14	2	0.18	Coarse marcasite rim
		6.1	0.45	Mean values for coarse-grained iron sulfide minerals
7	G6-25-47	73	2.0	Fine-grained marcasite
8	G6-25-47	600	15.0	Rim of marcasite aggregate
9	G6-25-47	99	9.2	
10	G7-16-14	100	3.7	Fine-grained pyrite with rim of microcrystalline pyrite
11	G7-16-14	54	1.7	Fine-grained marcasite
12	G7-16-14	155	2.1	Fine-grained marcasite
13	G7-16-14	72	4.1	Fine-grained marcasite in center of oolith
14	G7-16-14	180	10.0	Fine-grained marcasite in center of oolith
		167	6.0	Mean values for fine-grained iron sulfide minerals
15	G6-25-47	39	2.0	Fractured coarse pyrite with microcrystalline pyrite rim
16	G6-25-47	41	3.2	Coarse pyrite with visible rim of microcrystalline pyrite
17	G6-25-47	11	1.5	Fine-grained marcasite with euhedral marcasite rim
18	G6-25-47	35	1.5	Fine-grained marcasite with euhedral marcasite rim
19	G7-16-14	131	3.5	Medium-grained pyrite rimmed by microcrystalline pyrite
20	G7-16-14	28	1.9	Coarse pyrite with zoning
21	G7-16-14	35	0.5	Coarse pyrite with microcrystalline pyrite rim
22	G7-16-14	50	2.4	Factured coarse pyrite with microcrystalline pyrite rim and filling fractures
23	G7-16-14	98	2.3	Medium-grained euhedral pyrite with microcrystalline rim
		52	2.1	Mean values for mixed coarse- and fine-grained iron sulfide minerals

[1] G6-25-47 contains 6.7 g/mt (0.216 oz/t) gold; G7-16-14 contains 31.1 g/mt (1.002 oz/t) gold

SIMS analyses show that gold in the fine grains and rims ranged from 54 to 600 ppm (mean = 167 ppm; Table 2, analyses 7–14); arsenic ranged from 1.7 to 15 wt percent (mean = 6.0 wt %). As most gold-bearing grains or rims are much smaller than the analyzed spot, arsenic and gold are diluted by other phases in some analyses; however, results clearly demonstrate that significant gold resides in fine-grained pyrite and marcasite. In the remaining SIMS analyses (Table 2, analyses 15–23), mixtures of fine- and coarse-grained iron sulfide minerals were analyzed, resulting in intermediate values for gold and arsenic. Gold ranged from 11 to 131 ppm (mean = 52 ppm) and arsenic ranged from 0.5 to 3.5 wt percent (mean = 2.1 wt %).

Figure 6 documents the positive correlation between arsenic and gold in SIMS analyses (open diamonds). Because gold and arsenic correlate positively, X-ray maps of arsenic in pyrites with a variety of morphologies were generated. Maps show that small, ore-stage grains are unzoned and arsenic enriched. In rare instances, particularly where several grains coalesced, multiple arsenic-enriched zones were present.

Ore-stage grains and rims in five samples were analyzed for gold and other trace metals using EMPA (Table 1). Iron and sulfur are significantly below stoichiometric concentrations owing to substitution by other elements. Arsenic ranged from 3.1 to 11.3 wt percent and generally exceeded 5 wt percent; gold concentrations reached 2,400 ppm and commonly exceeded 200 ppm. Ore-stage grains and rims are also distinguished by consistently elevated copper, 0.09 to greater than 1 wt percent, and highly variable antimony, mercury, and thallium ranging from below detection limits to greater than 1 wt percent. These grains contained no detectable molybdenum or silver, and nickel, zinc, and tellurium varied from below to just above detection limits. Lead values are quite variable and ranged from below detection limits to, commonly, 0.2 wt percent. Approximately 0.05 wt percent cobalt is present, similar to preore pyrites. Arsenic and gold correlate positively, but gold/arsenic ratios are variable (Fig. 6). Concentrations determined by EMPA for both gold and arsenic extend to higher values than concentrations determined using SIMS. These results reflect decreased dilution by nonore pyrite in the smaller spots analyzed by the electron microprobe. Four analyses have unusually high gold/arsenic, with gold values reaching ~1,500 to 2,500 ppm (Fig. 6). Other than these four analyses, results are consistent with SIMS analyses.

Gold- and arsenic-bearing iron sulfide minerals are consistently concentrated along jasperoid grain boundaries or enclosed within jasperoid crystals (Fig. 5C). In rare instances, euhedral quartz crystals with growth zones contain ore-stage iron sulfide minerals indicating that the sulfide grains were trapped during quartz crystal growth in open space. The consistent association of gold-bearing pyrite and/or marcasite and jasperoid (Fig. 5C) indicates that they are contemporaneous minerals formed during a single stage of hydrothermal mineralization (Fig. 4).

Ore-stage jasperoid typically exhibits a reticulate texture, variable grain size, and abundant calcite inclusions, all of which indicate replacement of calcite (Fig. 5D; Lovering, 1972). Locally, where replacement was incomplete, calcite remains interstitial to quartz. The presence of growth zones delineated by solid calcite inclusions and the reticulate texture provide evidence for the deposition of silica as crystalline quartz rather than as silica gel and imply deposition at moderate,

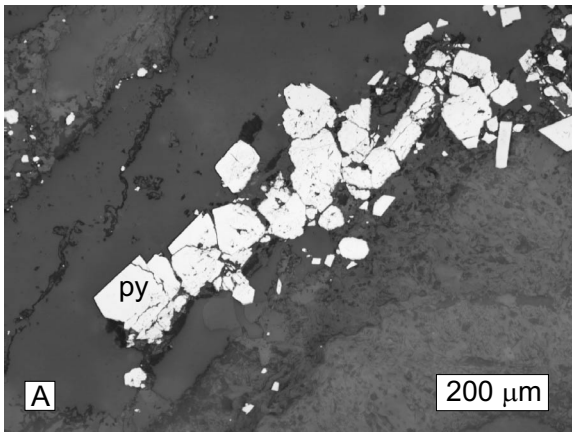
py
A
200 μm

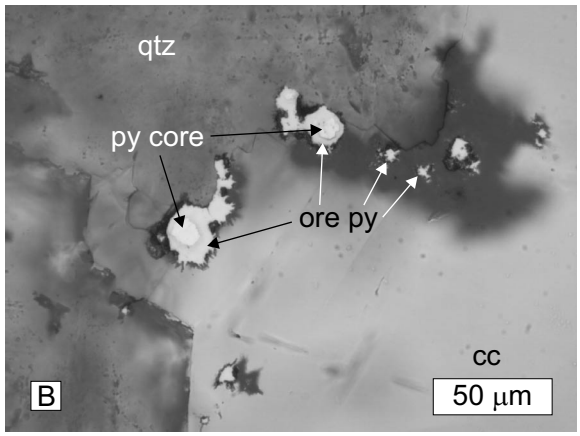
qtz
py core
ore py
cc
B
50 μm

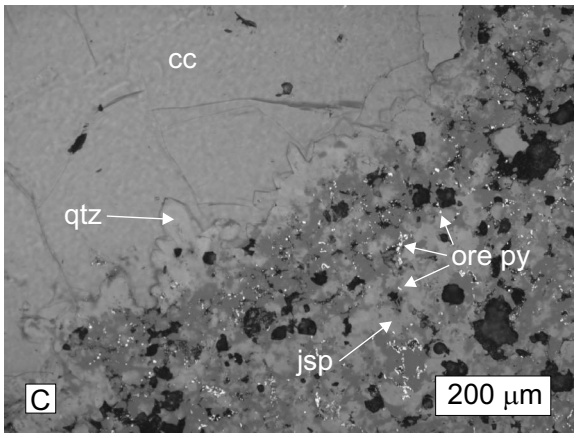
cc
qtz
ore py
jsp
C
200 μm

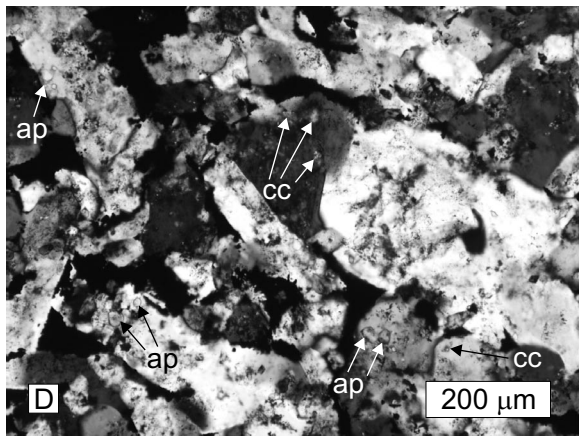
ap
cc
ap
ap
cc
D
200 μm

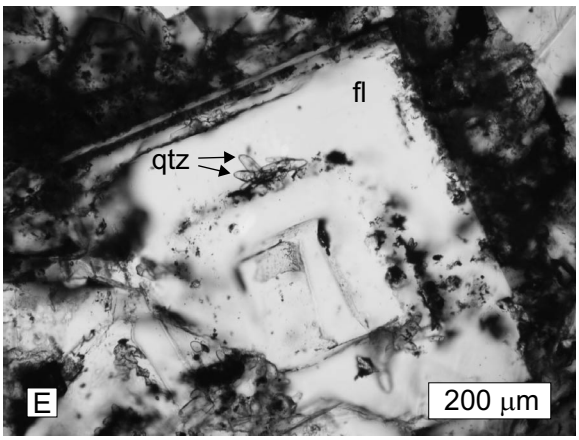
fl
qtz
E
200 μm

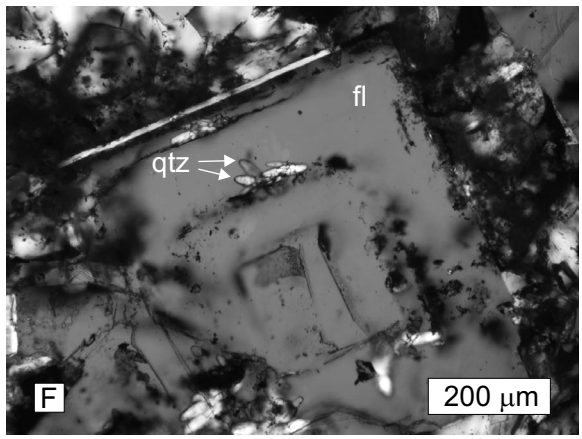
fl
qtz
F
200 μm

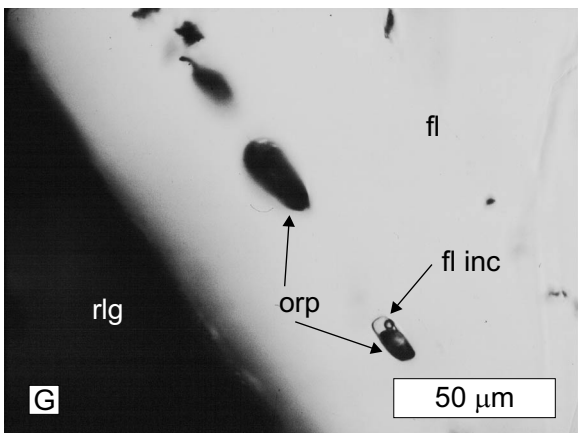
fl
fl inc
rlg
orp
G
50 μm

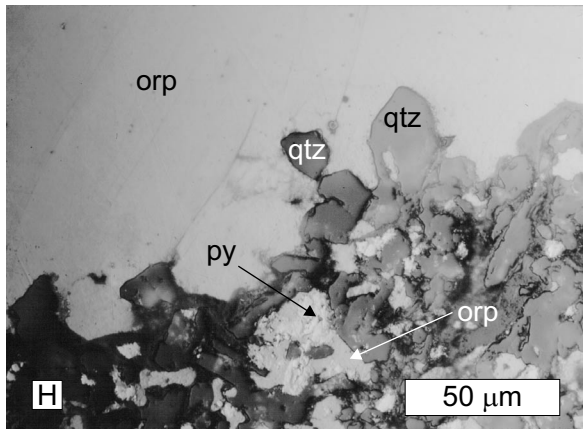
orp
qtz
qtz
py
orp
H
50 μm

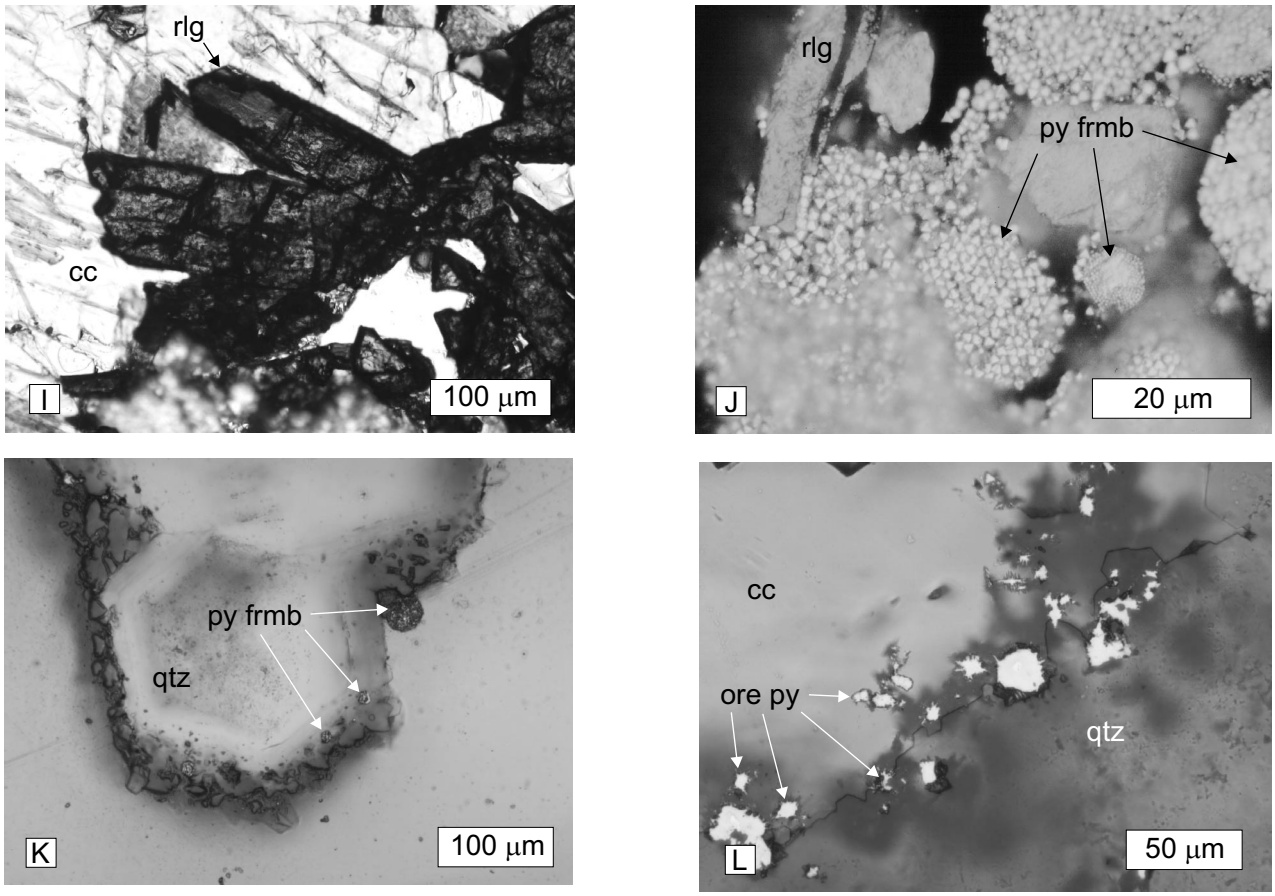

FIG. 5. Photomicrographs of preore, gold ore, and late gold ore-stage minerals. A. Moderately coarse, high-relief, and well-polished pregold vein pyrite. RPPL, sample GE 8304. B. Gold- and arsenic-enriched iron sulfide grains and rims on gold-free cores. RPPL, sample 92-118 42, 33.7 g/mt (1.084 oz/t) gold over 5-ft core interval. C. Typical ore-stage jasperoid with ore-stage iron sulfide minerals rimmed by euhedral quartz and overgrown by late ore calcite. Most iron sulfide minerals lie along jasperoid grain boundaries. Black regions are pore spaces. RPPL, sample 4820 186.5 5/6B, 30.1 g/mt (0.968 oz/t) gold. D. Typical jasperoid with calcite inclusions and detrital apatite. TXPL, sample GQR4, ~7.8 to 16.0 g/mt (~0.25–0.5 oz/t) gold. Transmitted plain (E) and crossed (F) polarized light images of intergrown cubic fluorite and fine euhedral quartz crystals along fluorite growth zones, showing temporal overlap of precipitation in open space. Sample GEFL-1A. G. Growth zone in euhedral fluorite crystal is defined by solid inclusions of orpiment, one of which is attached to a fluid inclusion. The fluorite was enclosed by realgar. TPPL, sample GEFL-1C. H. Intergrowth of crystalline quartz (dark to light gray), ore-stage pyrite (white, high relief), and orpiment (light gray, low relief) in lower part of photo is overgrown by massive orpiment. Quartz shows a range of gray shades owing to underlying orpiment. Textures show that vugs interstitial to euhedral quartz contain intergrown gold-bearing iron sulfide grains and orpiment. Massive orpiment is free of iron sulfide grains. RPPL, sample 92-196 231.8, 30.4 g/mt (0.978 oz/t) gold. I. Subhedral to euhedral realgar crystals encompassed by coarse calcite. TPPL, sample G7. J. Intergrown realgar crystals and pyrite framboids; tip of long realgar crystal (left center) encompasses a framboid crystallite as the framboid overgrows the realgar crystal, demonstrating contemporaneous precipitation. T and RPPL, sample G6-23-27, ~7.8 to 16.0 g/mt (~0.25–0.50 oz/t) gold. K. Cross section of euhedral quartz crystal that rims jasperoid mass. Core of crystal contains abundant primary fluid inclusions, which make the quartz appear dark and mottled. The crystal rim is decorated with intergrown framboidal pyrite and euhedral quartz crystals. Intergrown pyrite and realgar in (J) are from a similar rim. T and RPPL, sample G6-23-27, ~0.25 to 0.5 oz/t gold. L. Jasperoid rimmed by fine euhedral quartz crystals and overgrown by late ore-stage calcite. Iron sulfide minerals are enclosed by calcite adjacent to the quartz-calcite contact but diminish with distance from this contact. R and TPPL sample 92-118 42, 33.7 g/mt (1.084 oz/t) gold. Abbreviations: ap = apatite, cc = calcite, fl = fluorite, fl inc = fluid inclusion, frmb = framboid, jsp = jasperoid, orp = orpiment, py = pyrite, qtz = quartz, rlg = realgar, RPPL = reflected plane-polarized light, TXPL = transmitted crossed-polarized light, TPPL = transmitted plane-polarized light.

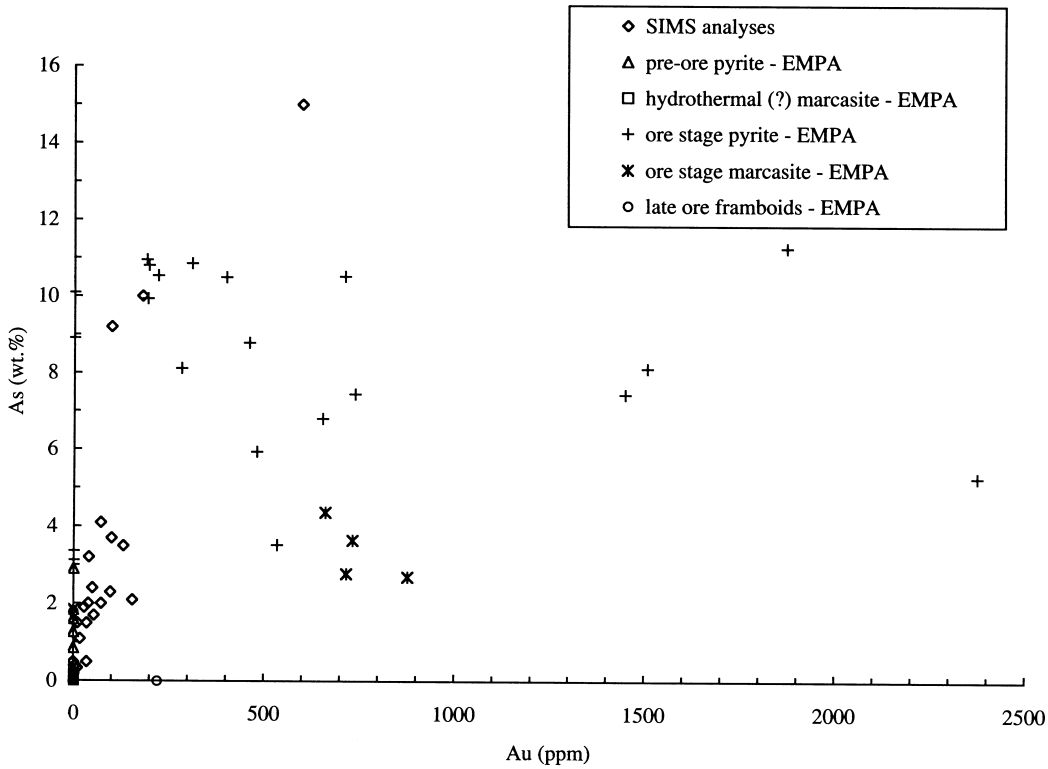

FIG. 6. Arsenic (wt %) and gold (ppm) in preore, gold ore, and late gold ore-stage iron sulfide minerals determined by SIMS and EMPA. As EMPA have higher detection limits than SIMS analyses, there are no EMPA points at low gold values. SIMS analyses indicating greater than about 50 ppm gold reflect analysis of fine-grained, gold ore-stage pyrite (see Table 2).

rather than low, temperatures. The presence of open space during jasperoid precipitation is indicated by the occurrence of small vugs and rinds of fine euhedral quartz crystals on masses of jasperoid and iron sulfide minerals (Fig. 5C). Although abundant open space was generated by faulting, the presence of small vugs with drusy quartz suggests that limestone dissolution and silica deposition were not always simultaneous and that dissolution created open space, subsequently filled or partly filled by fine euhedral quartz. Cathodoluminescence studies show that jasperoid crystals display a range of degrees of luminescence, demonstrating at least subtle changes in fluid composition as jasperoid was deposited.

Much jasperoid is unmineralized and lacks ore-stage iron sulfide minerals. Localized zoning of barren jasperoid to jasperoid plus ore-stage pyrite-marcasite is common. This zoning suggests that jasperoid formed before and possibly after gold and/or pyrite precipitation (Fig. 4). Some barren jasperoid contains coarse, irregular masses of marcasite grains. EMPA show that, although gold free, this marcasite contains low but anomalous arsenic as well as copper, antimony, and thallium (Table 1).

Rare, small blades and masses of intersecting blades of marcasite, which have high relief and are well polished, occur locally in the ore assemblage. The grains appear to have precipitated in open space or replaced calcite and were encompassed by jasperoid. Realgar is commonly spatially associated with this marcasite and overgrows jasperoid containing the marcasite. This spatial association suggests that the marcasite may have formed near the end of the ore stage and partially filled space created by limestone dissolution or faulting (Fig. 4). Remaining vugs were filled by realgar during the late ore stage. EMPA show that this bladed marcasite contains relatively low arsenic, 1.8 to 4.4 wt percent, but gold values reach 900 ppm (Table 1; Fig. 6). The marcasite blades also contain anomalous copper and variably anomalous antimony, mercury, and thallium, documenting an affinity with ore-stage mineralization.

Subhedral to euhedral fluorite is a rare component of the ore assemblage but was locally abundant in the south wall of the North pit (Fig. 2). More recently, minor fluorite has been documented in the Getchell Underground and Turquoise Ridge deposits (D. Tretbar and C. McAllister, pers. commun., 2000). Fluorite from the North pit commonly encompassed ore-stage jasperoid and drusy quartz and, less commonly, ore-stage iron sulfide minerals and orpiment (Fig. 4). Fine quartz crystals line growth zones in fluorite (Fig. 5E and F), indicating temporal overlap. The presence of euhedral fluorite crystals and crystals that terminate in vugs shows that fluorite precipitated in open space. This fluorite was recently dated using Th-Pb at 34 ± 11 Ma (Hofstra et al., 2000). The large error results from low thorium and the relatively young age of the fluorite, but, within the error, the age is consistent with ages determined for adularia at Twin Creeks (Groff et al., 1997; Hall et al., 1997).

Small, solid inclusions of orpiment locally define fluorite growth zones (Fig. 5G) and indicate that orpiment was a stable phase at the time fluorite precipitated (Fig. 4). Orpiment

inclusions are rare in jasperoid, suggesting that most orpiment precipitated after jasperoid encompassed most gold-bearing iron sulfide minerals. In a few high-grade samples, orpiment is intergrown with, or encompasses ore-stage iron sulfide minerals and euhedral to anhedral quartz. These intergrowths are locally rimmed by massive orpiment (Fig. 5H). The presence of massive orpiment encompassing ore-stage quartz and iron sulfide intergrowths, and fluorite and orpiment encompassing euhedral quartz crystal faces, demonstrates that fluorite and orpiment precipitated at the end of the ore stage (Fig. 4). Massive orpiment encompassing euhedral quartz crystals that rim jasperoid plus pyrite-bearing ore is also observed at Twin Creeks (Simon et el., 1999, see their fig. 4F).

Galkhaite, although not abundant, is locally common in underground workings in the Northwest ore zone below the North pit (D. Tretbar, pers. commun., 2000). Galkhaite observed during this study occurs as fine, cubic crystals in particularly vuggy ore horizons. The mineral conforms to drusy quartz crystals and terminates in vugs or is overgrown by late ore-stage realgar, indicating a paragenetic position similar to fluorite and orpiment. Galkhaite has recently been dated using Rb-Sr and gave an age of 39.0 ± 2.1 Ma (Tretbar et al., 2000), consistent with ages determined for fluorite at Getchell (Hofstra et al., 2000) and adularia at Twin Creeks (Groff et al., 1997; Hall et al., 1997).

Minor apatite is present in the gold ore assemblage, commonly as <15 μm, roughly spherical grains enclosed in jasperoid (Fig. 5D). Much jasperoid is free of apatite; however, in some high-grade zones, apatite may constitute as much as 5 vol percent of the assemblage. The erratic distribution and spherical form indicate that apatite is likely detrital and inherited from the sedimentary host rocks. The increased concentration of apatite in ore may reflect increased decalcification and concentration of insoluble materials, including both apatite and gold-bearing pyrite and/or marcasite.

Late ore mineralization

Realgar and calcite fill or partly fill vugs and larger open spaces and, with minor euhedral quartz, framboidal pyrite, and rare stibnite, form a late ore mineral assemblage that precipitated in open space (Fig. 5I). Coarse realgar typically forms overgrowths on or encompasses ore-stage minerals (Fig. 5G). Rare sprays of stibnite are encompassed by realgar. Significantly, in a few localities, realgar, in contact with ore-stage quartz containing gold-bearing pyrite and/or marcasite, encloses gold-bearing pyrite and/or marcasite. Realgar encloses iron sulfide grains only near quartz-realgar contacts; massive realgar is free of iron sulfide grains. Ore-stage iron sulfide minerals are locally enclosed by orpiment at Twin Creeks (Simon et al., 1999).

Rare pyrite framboids, some of which are intergrown with realgar (Fig. 5J), rim ore-stage euhedral quartz crystals or are partly incorporated in quartz crystal rims (Fig. 5K). These textures show that the outermost rims of some euhedral quartz crystals formed during the late ore stage (Fig. 5K) and also demonstrate a hydrothermal origin for the framboids. Two framboids analyzed using EMPA contain variable gold, arsenic, copper, thallium, and silver (Table 1), supporting their hydrothermal origin. Interestingly, they constitute two of only three iron sulfide grains that contain detectable silver.

Late ore-stage, coarse-grained, clear calcite commonly encloses realgar (Fig. 5I) and locally encloses earlier ore-stage minerals. This calcite precipitated last, conforms to euhedral crystal faces of earlier phases, and commonly fills remaining open space. Calcite is generally barren of gold mineralization; however, in some localities where calcite is in contact with ore-stage quartz, calcite contains ore-stage, iron sulfide minerals and carries significant gold values (Fig. 5L). As observed with realgar, ore-stage iron sulfide grains are only present in calcite adjacent to the ore-stage assemblage; they are not present in massive, coarse-grained calcite, distal from this contact.

Postore-stage(?) calcite

Coarse, translucent euhedral calcite crystals occur in fracture zones that are not spatially or genetically associated with earlier assemblages. The timing of this calcite is unconstrained, but it may be postore, similar to coarse calcite in open fractures at Meikle, dated using U-Pb at ~2 Ma (Emsbo, 1999; Hofstra et al., 2000).

Temporal Significance of the Mineral Paragenesis

Secondary hydrothermal minerals in the Getchell deposit document the occurrence of two or more hydrothermal events. Early quartz, pyrite, and base metal vein mineralization is spatially associated with the perimeter of the Late Cretaceous Osgood stock and is most likely associated with granodiorite intrusion. SIMS and EMPA and fire assays indicate that gold deposition did not accompany this event. Vein pyrite and quartz were fractured by at least one deformational event and cemented by ore-stage gold- and arsenic-enriched pyrite, quartz, and realgar.

Textural relationships strongly support the interpretation that gold mineralization and arsenic sulfide minerals precipitated during a single, evolving hydrothermal system, and that this hydrothermal event followed quartz and base metal vein mineralization. Chemical analyses and textural relationships indicate that gold was incorporated in arsenian pyrite and marcasite that form fine discrete grains, or form rims on earlier, gold-free pyrite. Gold-bearing iron sulfide grains are consistently encompassed by jasperoid that replaced limestone. This association indicates that either individual gold-bearing iron sulfide grains nucleated and precipitated on jasperoid and were encompassed by jasperoid as it continued to replace limestone, or isolated ore-stage iron sulfide grains precipitated, were present in the hydrothermal fluid, and were enclosed by jasperoid and/or were concentrated along the boundaries of jasperoid crystals as jasperoid precipitated. The first option requires precipitation of sulfide grains and jasperoid at about the same time. The second option permits a time lag between sulfide and jasperoid precipitation. In either case, the consistent spatial and textural relationships between arsenian, gold-bearing pyrite and jasperoid, lack of crosscutting features, and limited occurrence of gold-bearing iron sulfide minerals in later phases support the near-contemporaneous precipitation of gold-bearing iron sulfide minerals and jasperoid. The consistent presence of gold in pyrite or marcasite, ubiquitous presence of H_2S in ore fluids (indicated by quadruple mass spectrometer analyses), low salinities of ore

fluids, low base metal concentrations in ore-stage iron sulfide minerals (Table 1), and presence of gold-bearing pyrite and/or marcasite in jasperoid formed by fluid-rock reaction are consistent with gold deposition during sulfidation of reactive iron in the host rocks.

The presence of minor gold-bearing iron sulfide minerals in realgar and calcite, where these minerals are in contact with ore-stage jasperoid, is significant in that it shows that there is no major time break separating ore-stage and late ore-stage mineral deposition. The enclosure of fine, gold-bearing pyrite and/or marcasite by jasperoid, realgar, and calcite requires close timing for the precipitation of these minerals and contradicts an earlier interpretation that gold and arsenic sulfide precipitation were separated by 40 m.y. (Groff et al., 1997). It is conceivable that dissolution of jasperoid liberated some of the iron sulfide grains for later enclosure by realgar and calcite. However, this hypothesis is unsupported by textural evidence at Getchell and at other Carlin-type gold deposits (Hofstra and Cline, 2000). The lack of dissolution textures and the preservation of euhedral, ore-stage drusy quartz crystals separating jasperoid and calcite (Fig. 5L) or realgar argue against this alternative.

The continuous evolution of the gold ore stage to the late ore stage is further supported by the consistent successive overgrowth of younger minerals on perfectly preserved euhedral faces of older minerals (Fig. 5C, E, F, G, H, I, K, and L) and by fluid inclusion data that document a declining fluid temperature at constant salinity and gas content, for paragenetically successive minerals. The 180° to 240°C ore fluid initially reacted with and dissolved the limestone host rock and replaced the limestone with jasperoid and gold-bearing pyrite (Cline and Hofstra, 2000). In regions of open space generated by decalcification or earlier faulting, similar fluids with the same temperature, salinity, and gas content precipitated drusy quartz (Cline and Hofstra, 2000; Hofstra and Cline, 2000). Other minerals precipitated successively near the end of the ore stage and during the late ore stage from fluids with similar salinities and gas contents but at lower temperatures. Temperatures of 135° to 200° and ~175°C are indicated for precipitation of orpiment and fluorite, respectively. Orpiment, fluorite, and realgar precipitated in open space generated, primarily, by earlier movement on the Getchell fault. The precipitation of these minerals in open space and the documented lower temperatures are consistent with the sensitivity of the solubilities of these minerals to temperature (Hofstra et al., 1991; Hofstra, 1994) and demonstrate that these minerals precipitated as spent ore fluids cooled in open fractures. Late calcite probably precipitated at lower temperatures as near-surface fluids saturated in calcium carbonate descended into former upflow zones of the hydrothermal system during waning hydrothermal activity and became heated.

Related deposition of gold mineralization and the arsenic-rich, late ore stage is, finally, supported by the fact that these two assemblages occupy exactly the same region, northeast of the Osgood stock (Groff et al., 1997, their fig. 6). Gold mineralization is temporally related to the described ore- and late ore-stage minerals, and the ages determined for fluorite and galkhaite at Getchell and adularia at Twin Creeks indicate a mid-Tertiary age for gold deposition.

Acknowledgments

My sincere thanks to Bill Bagby, previously with the U.S. Geological Survey, for first involving me in the study of Getchell and Carlin-type gold deposits. I am especially indebted to Dick Nanna and the many employees at Getchell Gold Corporation for their assistance. In particular, Dick Nanna, Mark Gingrich, Mike Baumann, Dave Tretbar, and Judi Culver contributed to my understanding of the geology at Getchell. Mark Gingrich is thanked for providing a geologic map of the region around Getchell. Al Hofstra and Jim Reynolds continue to improve my understanding of Carlin gold systems and textural interpretations. Discussions with Bob Bodnar, Tracy Cail, Ray Donelick, Doug Goff, Jan Lamb, Carl "Tony" Kuehn, Charles McAllister, Michiko Shigehiro, and Kelli Weaver also contributed to this study. Comments by Tony Kuehn and an anonymous *Economic Geology* reviewer improved the manuscript. Todd Solberg and Mike Spilde are thanked for their assistance with EMPA, and Adam Merrill, Nick Wilson, and Joel Rotert helped generate figures. Funding for this study was provided by National Science Foundation grants EAR-9110587 and EAR-9305325 and the National Science Foundation EPSCoR WiSE program, grant 95-UNS-45. Getchell Gold Corporation provided gold analyses.

December 7, 1999; July 21, 2000

REFERENCES

Arehart, G.B., 1996, Characteristics and origin of sediment-hosted disseminated gold deposits: A review: Ore Geology Reviews, v. 11, p. 383–403.

Arehart, G.B., Chryssoulis, S.L., and Kesler, S.E., 1993a, Gold and arsenic in iron sulfides from sediment-hosted disseminated gold deposits: Implications for depositional processes: Economic Geology, v. 88, p. 171–185.

Arehart, G.B., Eldridge, C.S., Chryssoulis, S.L., and Kesler, S.E., 1993b, Ion microprobe determination of sulfur isotope variations in iron sulfides from the Post-Betze sediment-hosted disseminated gold deposit, Nevada, USA: Geochimica et Cosmochimica Acta, v. 57, p. 1505–1519.

Arehart, G.B., Foland, K.A., Naeser, C.W., and Kesler, S.E., 1993c, $^{40}Ar/^{39}Ar$, K/Ar, and fission track geochronology of sediment-hosted disseminated gold deposits at Post-Betze, Carlin Trend, northeastern Nevada: Economic Geology, v. 88, p. 622–646.

Armstrong, R.L., 1968, Sevier orogenic belt in Nevada and Utah: Geological Society of America Bulletin, v. 79, p. 429–458.

Bakken, B.M., and Einaudi, M.T., 1986, Spatial and temporal relations between wall rock alteration and gold mineralization, main pit, Carlin gold mine, Nevada, U.S.A., *in* Macdonald, A.J., ed., Gold '86: Willowdale, Ontario, Konsult Interantional, p. 388–403.

Bakken, B.M., Hochella, M.F., Jr., Marshall, A.F., and Turner, A.M., 1989, High-resolution microscopy of gold in unoxidized ore from the Carlin mine, Nevada: Economic Geology, v. 84, p. 171–179.

Burchfiel, B.C., Cowan, D.S., and Davis, G.A., 1992, Tectonic overview of the Cordilleran orogen in the western United States, *in* Burchfiel, B.C., Lipman, P.W., and Zoback, M.L., eds., The Cordilleran orogen: Conterminous U.S.: Geological Society of America, Geology of North America, v. G-3, p. 407–479.

Cail, T., 1999, Alteration associated with gold deposition at the Getchell, Carlin-type gold deposit, north-central Nevada: Unpublished M.Sc. thesis, Las Vegas, University of Nevada, 184 p.

Christensen, O.D., 1995, Carlin Trend geologic overview: Society of Economic Geologists Guidebook Series, v. 8, p. 12–26.

Chryssoulis, S.L., 1990, Detection and quantification of "invisible" gold by microprobe techniques, *in* Hausen, D.M., ed., Gold '90: New York, Society of Mining Engineers, p. 323–332.

Chryssoulis, S.L., Cabri, L.J., and Salter, R.S., 1987, Direct determination of invisible gold in refractory sulphide ores, *in* Salter, R.S., Wyslouzil, D.M., and McDonald, G.W., eds., Proceedings international symposium on gold metallurgy—refractory gold: Oxford, England, Pergamon Press, p. 235–244.

Cline, J.S., and Hofstra, A.H., 2000, Ore fluid evolution at the Getchell Carlin-type gold deposit, Nevada, USA: European Journal of Mineralogy, v. 12, p. 195–212.

Drews-Armitage, S.P., Romberger, S.B., and Whitney, C.G., 1996, Clay alteration and gold deposition in the Genesis and Blue Star deposits, Eureka County, Nevada: ECONOMIC GEOLOGY, v. 91, p. 1383–1393.

Emsbo, P., 1999, Origin of the Meikle high grade gold deposit from the superposition of Late Devonian Sedex and mid-Tertiary Carlin-type gold mineralization: Unpublished Ph.D. thesis, Golden, Colorado, Colorado School of Mines, 394 p.

Emsbo, P., Hofstra, A.H., Park, D., Zimmerman, J.M., and Snee, L., 1996, A mid-Tertiary age constraint on alteration and mineralization in igneous dikes on the goldstrike property, Carlin Trend, Nevada [abs.]: Geological Society of America Abstracts with Programs, v. 28, no. 7, p. A-476.

Folger, H.W., Snee, L.W., Mehnert, H.H., Hofstra, A.H., and Dahl, A.R., 1996, Significance of K-Ar and $^{40}Ar/^{39}Ar$ dates from mica in Carlin-type gold deposits: Evidence from the Jerritt Canyon district, Nevada: Geology and Ore Deposits of the American Cordillera Symposium, Geological Society of Nevada, Reno-Sparks, Nevada, Proceedings, p. 41–60.

Groff, J.A., 1996, ^{40}Ar-^{39}Ar geochronology of gold mineralization and origin of aurifereous fluids for the Getchell and Twin Creeks mines, Humboldt County, Nevada: Unpublished Ph.D. thesis, Socorro, New Mexico Institute of Mining and Technology, 291 p.

Groff, J.A., Heizler, M.T., McIntosh, W.C., and Norman, D.I., 1997, $^{40}Ar/^{39}Ar$ dating and mineral paragenesis for Carlin-type gold deposits along the Getchell Trend, Nevada: Evidence for Cretaceous and Tertiary gold mineralization: ECONOMIC GEOLOGY, v. 92, p. 601–622.

Hall, C.M., Simon, G., and Kesler, S.E., 1997, Age of mineralization at the Twin Creeks SHMG deposit, Nevada: Society of Economic Geologists Guidebook Series, v. 28, p. 151–154.

Hausen, D.M., and Kerr, P.F., 1968, Fine gold occurrence at Carlin, Nevada, *in* Ridge, J. D., ed., Ore deposits in the United States 1933-1967 (Graton-Sales Volume): New York, Society of Mining Engineers, AIME, p. 909–940.

Hobbs, S.W., 1948, Geology of the northern part of the Osgood Mountains, Humboldt County, Nevada: Unpublished Ph.D. thesis, New Haven, Connecticut, Yale University.

Hofstra, A.H., 1994, Geology and genesis of the Carlin-type gold deposits in the Jerritt Canyon district, Nevada: Unpublished Ph.D. thesis, Boulder, CO, University of Colorado, 719 p.

Hofstra, A.H., and Cline, J.S., 2000, Characteristics and models for Carlin-type gold deposits: Reviews in Economic Geology, v. 13, p. 163–220.

Hofstra, A.H., Leventhal, J.S., Northrop, H.R., Landis, G.P., Rye, R.O., Birak, D.J., and Dahl, A.R., 1991, Genesis of sediment-hosted disseminated-gold deposits by fluid mixing and sulfidization: Chemical-reaction-path modeling of ore-depositional processes documented in the Jerritt Canyon district, Nevada: Geology, v. 19, p. 36–40.

Hofstra, A.H., Snee, L.W., Rye, R.O., Folger, H.W., Phinisey, J.D., Loranger, R.J., Dahl, A.R., Naeser, C.W., Stein, H.J., and Lewchuk, M., 1999, Age constraints on Jerritt Canyon and other Carlin-type gold deposits in the western United States: Relationship to Mid-Tertiary extension and magmatism: ECONOMIC GEOLOGY, v. 94, p. 769–802.

Hofstra, A.H., Premo, W.R., Emsbo, P., Cline, J.S., and Aleinikoff, J.N., 2000, U-Th-Pb dating of hydrothermal minerals from Carlin-type gold deposits, Nevada—results and evaluation [ext. abs.]: Geology and Ore Deposits 2000: The Great Basin and Beyond, Geological Society of Nevada, Reno, Nevada, Program with Abstracts, p. 55.

Hotz, P.E., and Willden, R., 1964, Geology and mineral deposits of the Osgood Mountains quadrangle, Humboldt County, Nevada: U.S. Geological Survey Professional Paper 431, 128 p.

Jewell, P.W., and Parry, W.T., 1987, Geology and hydrothermal alteration of the Mercur gold deposit, Utah: ECONOMIC GEOLOGY, v. 82, p. 1958–1966.

Joralemon, P., 1951, The occurrence of gold at the Getchell mine, Nevada: ECONOMIC GEOLOGY, v. 46, p. 267–310.

Kuehn, C.A., and Rose, A.W., 1995, Carlin gold deposits, Nevada: Origin in a deep zone of mixing between normally pressured and overpressured fluids: ECONOMIC GEOLOGY, v. 90, p. 17–36.

Lamb, J., 1995, A petrographic and fluid inclusion study of the Purple Vein and post-Betze orebodies, Carlin, Nevada; Unpublished M.S. thesis, Las Vegas, Nevada, University of Las Vegas, 126 p.

Lovering, T.G., 1972, Jasperoid in the United States—its characteristics, origins, and economic significance: U. S. Geological Survey Professional Paper 710, 164 p.

Nanna, D., Baumann, M., Berentsen, E., and Steinman, G., 1987, Getchell deposit, *in* Johnson, J.L., ed., Bulk mineable precious metal deposits, guidebook for field trips: Reno, Nevada, Geological Society of Nevada, p. 353–356.

Nevada Bureau of Mines and Geology, 1999, Nevada geology: Newsletter 36, 4 p.

Oldow, J.S., 1984, Evolution of a late Mesozoic back-arc fold and thrust belt, north-western Great Basin, USA: Tectonophysics, v. 102, p. 245–274.

Pitkin, J.A., 1991, Radioelement data of the Getchell Trend, Humboldt County, Nevada—geologic discussion and possible significance for gold exploration, *in* Raines, G.L., Lisle, R.E., Schafer, R.W., and Wilkinson, W.H., eds., Geology and ore deposits of the Great Basin. Symposium proceedings: Reno, Nevada, Geological Society of Nevada, p. 759–770.

Radtke, A.S., 1985, Geology of the Carlin gold deposit: U.S. Geological Survey Professional Paper 1267, 124 p.

Ressel, M.W., Noble, D.C., and Connors, K.A., 1998, Eocene dikes of the Carlin Trend, Nevada: Magmatic As, Sb, Cs, Tl, CO_2 and excess Ar suggest a deep degassing model for gold mineralization: Geological Society of America Abstracts with Programs, v. 30, p. A-126.

Ressel, M.W., Noble, D.C., Henry, C.D., and Trudel, W.S., 2000, Dike-hosted ores of the Beast deposit and the importance of Eocene magmatism in gold mineralization of the Carlin Trend, Nevada: ECONOMIC GEOLOGY, v. 95, p. 1417–1444.

Silberling, N.J., and Roberts, R.J., 1962, Pre-Tertiary stratigraphy and structure of northwest Nevada: Geological Society of America Special Paper 72, 58 p.

Silberman, M.L., Berger, B.R., and Koski, R.A., 1974, K-Ar age relations of granodiorite emplacement and tungsten and gold mineralization near the Getchell mine, Humboldt County, Nevada: ECONOMIC GEOLOGY, v. 69, p. 646–656.

Simon, G., Kesler, S.E., and Chryssoulis, S., 1999, Geochemistry and textures of gold-bearing arsenian pyrite, Twin Creeks, Nevada: Implications for deposition of gold in Carlin-type deposits: ECONOMIC GEOLOGY, v. 94, p. 405–421.

Stenger, D.P., Kesler, S.E., Fortuna, J., and Peltonen, D.R., 1998, Role of sulfidation in deposition of gold, Twin Creeks sediment-hosted micron gold deposit, Nevada: Society of Economic Geologists Guidebook Series, v. 28, p. 147–150.

Stewart, J.H., 1980, Geology of Nevada: Nevada Bureau of Mines and Geology Special Publication 4, 136 p.

Tretbar, D.R., Arehart, G.B., and Christensen, J.N., 2000, Dating gold deposition in a Carlin-type gold deposit using Rb/Sr methods on the mineral galkhaite: Geology, v. 28, p. 947–950.

Wells, J.D., and Mullens, T.E., 1973, Gold-bearing arsenian pyrite determined by microprobe analysis, Cortez and Carlin gold mines, Nevada: ECONOMIC GEOLOGY, v. 68, p. 187–201.

Wilson, P.N., and Parry, W.T., 1995, Characterization and dating of argillic alteration in the Mercur gold district, Utah: ECONOMIC GEOLOGY, v. 90, p. 1197–1216.